Impact of metal artefacts due to EEG electrodes in brain PET/CT imaging

Catherine Lemmens[1], Marie-Louise Montandon[2], Johan Nuyts[1], Osman Ratib[2], Patrick Dupont[1,3] and Habib Zaidi[2]

[1]Department of Nuclear Medicine and Medical Imaging Center, University Hospital Gasthuisberg and Katholieke Universiteit Leuven, Leuven, Belgium
[2]Division of Nuclear Medicine, Geneva University Hospital, CH-1211 Geneva, Switzerland
[3]Laboratory for Cognitive Neurology, Katholieke Universiteit Leuven, Leuven, Belgium

For correspondence or reprints contact: Catherine Lemmens, M Sc., Herestraat 49, 3000 Leuven, Belgium, E-mail: catherine.lemmens@uz.kuleuven.be, tel: +32 16349085, fax: +32 16343759

Abstract
The goal of this study is to investigate the impact of EEG electrodes on the visual quality and quantification of ^{18}F-FDG PET images in neurological PET/CT examinations. For this purpose, the scans of twenty epilepsy patients with EEG monitoring were used. The CT data were reconstructed with filtered back projection (FBP) and with a metal artefact reduction (MAR) algorithm. Both data sets were used for CT-based attenuation correction (AC) of the PET data. Also, a calculated AC (CALC) technique was considered. A VOI and voxel-based quantitative analysis were performed to compare the different AC methods. Images were also evaluated visually by two observers. It was shown with simulations and phantom measurements that from the considered AC methods, the MAR-AC can be used as the reference in this setting. The visual assessment of PET images showed local hot spots outside the brain corresponding to the locations of the electrodes when using FBP-AC. In the brain, no abnormalities were observed. The quantitative analysis showed a very good correlation between PET-FBP-AC and PET-MAR-AC, with a statistically significant positive bias in the PET-FBP-AC images of about 5-7% in most brain voxels. There was also a good correlation between PET-CALC-AC and PET-MAR-AC but in the PET-CALC-AC images regions with both a significant positive and negative bias were observed. EEG electrodes give rise to local hot spots outside the brain and a positive quantification bias in the brain. However, when diagnosis is made by mere visual assessment, the presence of EEG electrodes does not seem to alter the diagnosis. When quantification is performed, the bias becomes an issue especially when comparing brain images with and without EEG monitoring.

Keywords: PET/CT, brain imaging, attenuation correction, metal artefacts, quantification.

1. Introduction

During the last decade, Positron Emission Tomography (PET) has worked its way into daily clinical routine. PET has become the imaging modality of choice for diagnosis, staging and restaging, and follow-up in oncology. In neurology, PET is steadily gaining importance both in clinical and research settings. Brain PET imaging enables *in vivo* visualization of cerebral blood flow, brain metabolism and neuroreceptor binding. To obtain quantitative PET images, the acquired projection data have to be corrected for photon attenuation, which has long been recognized as the most important physical degrading factor resulting in the loss of quantification ability (Zaidi *et al* 2007). In standalone PET, patient-specific attenuation correction factors (ACF) are usually obtained by acquiring a transmission scan using external positron-emitting (^{68}Ga/^{68}Ge) or single-photon (^{137}Cs) emitting radionuclide sources. Transmission scanning increases the total examination time considerably and produces a noisy attenuation map. In brain PET imaging, one can make use of alternative methods to obtain the attenuation map including calculated (Siegel and Dahlbom 1992; Weinzapfel and Hutchins 2001) and atlas-guided (Stodilka *et al* 2000; Montandon and Zaidi 2005; Zaidi *et al* 2004) methods. Numerous publications reported on the comparative assessment of a variety of attenuation correction strategies in brain PET imaging (Zaidi *et al* 2004; Zaidi *et al* 2007).

With the advent of combined PET/CT, the CT images are used for attenuation correction of the PET data. This eliminates the need for a lengthy transmission scan and results in an attenuation map with reduced noise. However, in the presence of high density material, like metals, the CT images contain streak artefacts. These artefacts may propagate into the PET images during the CT-based attenuation correction procedure, thus disturbing the visual interpretation and influencing the quantitative analysis (Goerres *et al* 2003; Kamel *et al* 2003; Ay and Zaidi 2006). Metal artefact reduction (MAR) algorithms have been developed to reduce the artefacts in CT imaging (Kalender *et al* 1987; Mahnken *et al* 2003; Lemmens *et al* 2006; Lemmens *et al* 2008). In PET/CT, MAR algorithms could be useful to restore the tracer concentration in the PET images.

In neurological PET/CT, epilepsy patients often receive electroencephalogram (EEG) monitoring during their examination. However, metallic EEG electrodes will cause artefacts in the CT images and thereby affect the PET images. In this study, the impact of the electrodes on the visual quality and the quantification of brain PET images is investigated. To this end, PET images corrected for attenuation using the standard (artefactual) CT images are compared to PET images corrected for attenuation using CT images reconstructed with a MAR algorithm. In addition, a comparison is made with an automated calculated attenuation correction technique using a three-tissue model (brain tissue, skull and scalp).

2. Methods and materials

2.1 Patient data acquisition

Twenty epilepsy patients with EEG monitoring were referred to the Nuclear Medicine Division of Geneva University Hospital for a PET scan for pre-surgical evaluation of epilepsy using [^{18}F]-Fluorodeoxyglucose (FDG). Their age ranged from 6 to 61 years (mean±SD = 26.10±14.76). The EEG Genuine Grass Precious Gold Disc Electrodes used in this study were supplied by Astro-Med, Inc. (West Warwick, RI, USA). The 32 electrodes used to record the EEG signal were carefully positioned according to the standard 10/20 system. PET/CT data acquisition was performed on a Biograph Sensation 16 (Siemens Medical Solutions, Erlangen, Germany) using a standard protocol recommended by the manufacturer. The PET acquisition was started approximately 30 min after injection of 370 MBq of [^{18}F]-FDG. The PET emission study (20 min, 1 bed position) followed immediately the CT study used for attenuation correction. Diagnostic quality CT imaging was performed under standard conditions (140 kVp, 320 mAs, 16×0.75 collimation, a pitch of 0.8 and 1.5 sec per rotation).

2.2 Phantom data acquisition

On clinical CT scanners, the maximum CT number in the CT images is 3071 Hounsfield units (HU) except when an extended CT scale is used (Coolens and Childs 2003). This means all

metallic objects will be set to 3071 HU, which underestimates their true HU. However, even when the extended CT scale would be used, the current conversion methods would result in incorrect PET attenuation values for metallic objects. If these CT images are used for attenuation correction of the PET images, lines of response (LORs) passing through metallic objects will be wrongly corrected. Therefore, two phantom experiments were conducted in order to estimate the effective attenuation coefficient of the electrodes at 511 keV. A uniform cylindrical phantom (22 cm diameter, wall thickness 6 mm) containing 8.6 MBq ^{68}Ge/^{68}Ga, and a large plastic water bottle (16 cm diameter, wall thickness 0.6 mm) containing 23 MBq [^{18}F]-FDG homogenously distributed throughout the water were used. To both phantoms eight EEG electrodes were attached on a single plane. A CT scan (140 kVp, 140 mAs, 16×0.75 collimation, a pitch of 0.8 and 0.75 sec per rotation) and PET scan (1 bed position of 30 min) were acquired for each phantom on the Biograph 16 PET/CT system at the KULeuven (which is the same system model as the one described above). A transaxial slice of the reconstructed PET images, unaffected by the electrodes, was selected to serve as the reference slice. The optimal attenuation coefficient of the electrodes at 511 keV was defined as the value for which the sum of squared differences between the artefactual PET slice with electrodes and the reference PET slice was minimized. In addition to this, it was checked whether this optimal attenuation coefficient also gave rise to the lowest standard deviation for a large region of interest in the artefactual slice (Stodilka *et al* 1998).

2.3 Simulation studies

Two computer simulation studies were performed to confirm the results obtained in the physical experiment. The first simulation reproduced the first phantom experiment described above. For the second simulation, one transaxial CT and brain PET image set of a patient without EEG monitoring was selected from the database. This patient had a normal distribution of [^{18}F]-FDG throughout the brain. Using these clinical data as input, CT and PET projection data were generated for a single slice, using analytical simulators and afterwards reconstructed. Then, a second simulation was performed by adding six golden electrodes to the CT reference image (CT-REF) and again CT and PET images were reconstructed using the second data set. The CT simulation software takes into account the finite size of the focus and the detector elements, the energy spectrum and the blurring due to rotation (De Man *et al* 1999).

2.4 Reconstruction of CT and PET data

The CT data were rebinned from 3D cone beam into 2D parallel beam configuration and then reconstructed twice at PET resolution (336x336 pixels). The first CT reconstruction was performed using conventional filtered back projection (FBP), which gave rise to typical artefactual images owing to presence of metals in the field of view. At CT resolution (512x512 pixels), our FBP reconstruction produces images very similar to the clinical images. The second reconstruction used the MAR algorithm described by Lemmens et al (2008). The algorithm starts with an initial reconstruction performed with a Maximum-Likelihood algorithm for Transmission tomography (MLTR) (De Man *et al* 1999). Based on this initial reconstruction, a label image is created on which multi-modal priors (Liang *et al* 1991; Nuyts *et al* 1999) are defined. Using these priors a Maximum-A-Posteriori (MAP) reconstruction is performed in order to obtain an artefact-free starting image (De Man *et al* 2000). This starting image is the basis for an image-based projection completion procedure in which the original metal projections are replaced by artificial projections. In the last step of the algorithm, the final reconstruction is obtained by using the corrected dataset and MLTR. The metal pixels in the MAR CT images are assigned appropriate attenuation coefficients based on the results of the phantom experiments described above.

After reconstruction, the CT images were visually compared for spatial alignment with the PET images reconstructed without attenuation correction (PET-NO-AC). In the case of visual mismatch between the two sets, the CT image was rigidly registered to the PET-NO-AC using an automated mutual information-based registration procedure (Maes *et al* 1997) to compensate for patient movement between the two scans. Before conversion to attenuation maps, the CT images were Gaussian smoothed using a full width at half maximum (FWHM) of 7 mm, which

is the value applied by the scanner manufacturer. The conversion was performed using a bilinear tube voltage-dependent scaling method (Carney *et al* 2006).

For the calculated attenuation map, the contour of the head was automatically derived from the emission sinogram using a method described by Ghoorun *et al* (2006). The method starts by low pass filtering the sinogram and setting all pixels having an intensity below a (very small) threshold to 1. This sinogram is backprojected to produce an image that contains for every pixel the fraction of projection lines with (nearly) zero count. A threshold is applied to this image to generate the head contour. This method is effective if most projection lines intersecting the head contour yielded a count rate significantly higher than zero. Based on our experience, the technique is robust and reliable for ^{18}F-FDG brain imaging.

A skull with a fixed thickness of 5 mm (Siegel and Dahlbom 1992) was added at a depth of 10 mm from the external contour of the head. The depth was derived from an adult patient in our sample. The attenuation coefficients at 511 keV used for brain (and scalp) tissue and skull were calculated using photon cross section data from the XCOM library (Hubbel J H, Seltzer S M Tables of X-Ray Mass Attenuation Coefficients and Mass Energy-Absorption Coefficients, NISTIR 5632 http://physics.nist.gov/PhysRefData/XrayMassCoef/cover.html) resulting in values of 0.099 cm^{-1} and 0.156 cm^{-1}, respectively. The attenuation of the head holder was taken into account by manually delineating the head holder in the CT images and repositioning it into the calculated attenuation map after appropriate scaling to 511 keV.

The 3D PET sinograms were corrected for detector sensitivity, dead time, random coincidences, scatter (Watson 2000) and attenuation, and converted to 2D sinograms using Fourier rebinning (Defrise *et al* 1997). For reconstruction, the sinograms were "uncorrected" for attenuation, and reconstructed with (attenuation weighted) Maximum-Likelihood Expectation Maximization (MLEM), accelerated using a gradually decreasing number of subsets (Hudson and Larkin 1994). The resolution of the PET images was further enhanced by incorporating a spatially invariant point spread function in the projector (5 mm FWHM, the spatial resolution near the center of the PET system) which also reduced the noise in the images (Zeng *et al* 1991).

For each patient, three PET attenuation corrected images were obtained: one PET image corrected with the CT-FBP reconstruction (PET-FBP-AC), PET corrected with the CT-MAR reconstruction (PET-MAR-AC) and PET corrected with the calculated attenuation (PET-CALC-AC).

2.5 Qualitative and quantitative image analysis

Qualitative image assessment was performed by two independent observers (experienced nuclear medicine physicians) that blindly assessed visually the images reconstructed using the three different protocols. Transaxial, sagittal and coronal slices were displayed without any identification besides a code not known by the 2 observers involved in the evaluation. Each observer was asked to assess overall image quality and instructed to indicate any visible artefacts or unexpected abnormalities that could be attributed to unsatisfactory reconstruction.

Reconstructed PET images using the three attenuation correction methods (PET-FBP-AC, PET-MAR-AC, and PET-CALC-AC) were also quantitatively analyzed using *BRASS*™ automated functional brain analysis software (Hermes *BRASS* software, Nuclear Diagnostics AB, Sweden). Briefly, *BRASS* fits and compares patient images to 3D reference templates created from images of healthy subjects (Slomka *et al* 2001). The three PET attenuation corrected images were nonlinearly warped (Radau *et al* 2001) individually to the *BRASS* template, which consist of a total of 63 defined regions, for an automated volume of interest (VOI)-based analysis. The correlation between mean activity concentration estimates obtained when using the three attenuation correction methods was checked on a VOI by VOI basis and using pooled VOI analysis. The means, standard errors and standard deviations of activity concentration estimates from clinical PET images reconstructed using the three attenuation correction techniques were compared. The relative difference was used as a figure of merit for comparative assessment both within subject and as group consisting of a homogenous sample.

In addition to the VOI-based analysis, a voxel-based analysis using statistical parametric mapping (Wellcome Department of Cognitive Neurology, London, UK

http://www.fil.ion.ucl.ac.uk/spm/ version SPM2) was performed. For each subject, images were nonlinearly warped into a common coordinate (MNI - Montreal Neurological Institute) space and smoothed using an isotropic 3D Gaussian kernel (FWHM=12 mm). Condition effects were estimated according to the general linear model at each voxel. Statistical threshold was set at $p < 0.05$ (Family-Wise Error (FWE) corrected). The following subtractions were performed: PET-FBP-AC – PET-MAR-AC and PET-CALC-AC – PET-MAR-AC (and vice versa). A map of the mean percentual difference between the different methods of reconstruction was also calculated to estimate the size of the difference using the PET-MAR-AC reconstruction as the reference.

3. Results

3.1 Phantom and simulation studies

Both phantom studies showed that a zero attenuation value should be assigned to the pixels identified as metallic EEG electrodes. Figure 1 shows the PET reconstructions for some of the tested linear attenuation coefficients for the electrodes in the water bottle experiment. The sum of squared differences (SSQD) and the standard deviation (SD) values are also given. Both metrics as well as the visual comparison of the PET images demonstrate that a zero attenuation value is optimal. The zero attenuation value was confirmed in the first simulation study. The MAR algorithm clearly reduces the streak artefacts due to the metallic electrodes. However, some residual heightened attenuation remains near the pixels which were considered to be metallic electrodes (set to zero attenuation) (figure 2C)
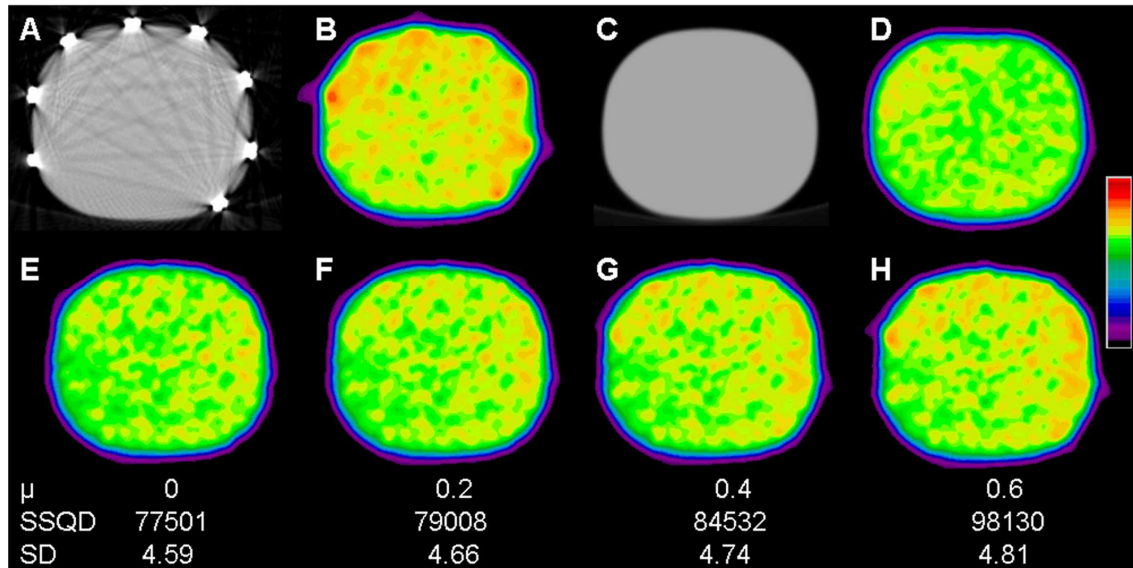

μ	0	0.2	0.4	0.6
SSQD	77501	79008	84532	98130
SD	4.59	4.66	4.74	4.81

Figure 1. Reconstructions of the water bottle phantom measurement. A) CT FBP reconstruction of a slice with electrodes, B) PET-FBP-AC reconstruction of a slice with electrodes, C) CT FBP reconstruction of the reference slice, D) PET-FBP-AC reconstruction of the reference slice. E-H) PET-MAR-AC reconstructions using different attenuation values (μ) for the EEG electrodes: E) μ = 0, F) μ = 0.2, G) μ = 0.4, and H) μ = 0.6. The sum of squared differences (SSQD) and the standard deviation values (SD) are also shown.
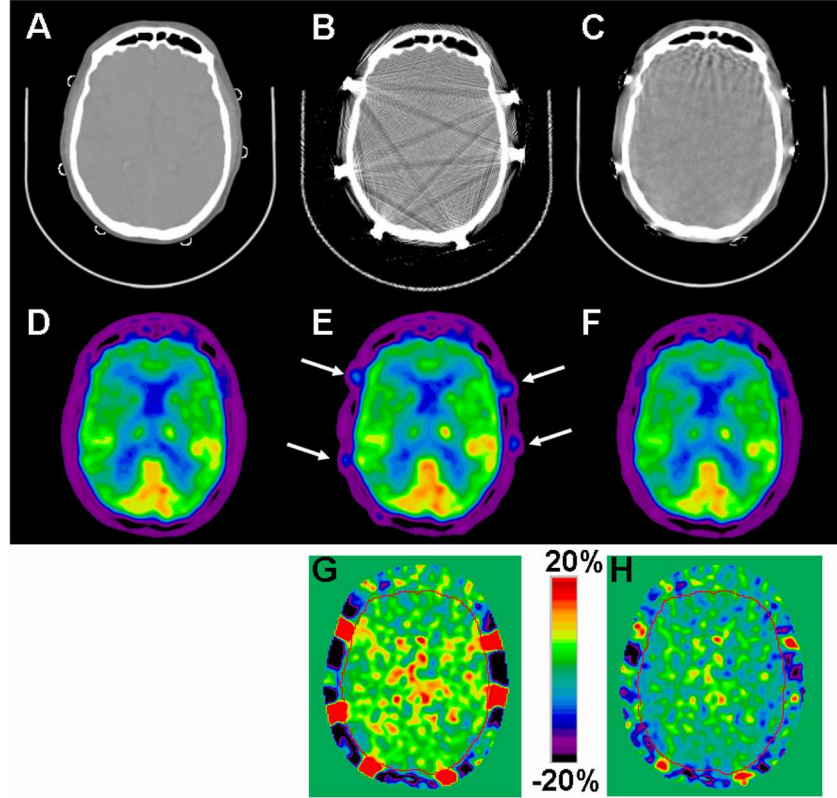
Figure 2. Reconstructions from the second simulation study. The top row shows the CT images whereas the middle and bottom rows show the corresponding PET and difference images. A) The CT reference image with electrodes, B) the CT FBP reconstruction, C) the CT MAR reconstruction with the electrodes set to zero attenuation, D) the PET reconstruction of the simulation without the electrodes (PET-REF), E) PET-FBP-AC, F) PET-MAR-AC, G) the relative difference image of PET-FBP-AC and PET-REF , and H) the relative difference image of PET-MAR-AC and PET-REF. The red contour is the delineation of the brain. The white arrows indicate some of the visible hot spot artefacts.

The qualitative visual assessment (figure 2) showed that the PET-FBP-AC image suffers from artefacts corresponding to the location of the electrodes (indicated by the white arrows). These artefacts disappear in the PET-MAR-AC image. The difference images (figure 2 G-H) revealed that the extent of the artefacts is not confined to the location of the electrodes as the tracer uptake is overestimated with PET-FBP-AC in the brain with 3.9 ± 4.5 % (max. 30, min -9). The tracer uptake in the brain is slightly underestimated by -0.7 ± 4.0 % (max. 19, min -13) when using PET-MAR-AC. These observations were also noted in the phantom experiments: For the slices affected by the metallic electrodes, PET-FBP-AC overestimated the activity concentrations inside the artefactual slices by 4 to 5% with respect to the activity inside the reference slices. With the PET-MAR-AC reconstructions of the phantoms, the activity concentrations of the slices affected by the metallic electrodes deviated by less than 1% from the activity concentrations inside the reference slices. This indicates that it is justified to use the PET-MAR-AC reconstruction as the reference in the further analysis.

3.2 Patient data processing
A cause for additional artefacts in PET is patient movement between the CT and PET data acquisition. Therefore, to avoid these additional effects, the CT and PET images were visually checked for any motion. In patient 3, substantial motion was detected and the CT images had to be registered rigidly to the PET-NO-AC image.

3.3 Qualitative visual assessment

An example of a reconstructed slice (of the data of one of the patients) using the three different methods is shown in figure 3. However, for the visual assessment, observers were looking only at the PET reconstructions using a 3D viewer. There was excellent concordance between both observers in terms of reporting the appearance of hot-spot artefacts in the FBP-CT attenuation corrected PET images, resulting from overcorrection of dense metallic electrodes. As a rule of thumb, examination of the non-attenuation corrected images in clinical routine was recommended to distinguish technical artefacts from physiologic/pathologic abnormalities (Kinahan *et al* 2003). These artefacts disappeared when using MAR-CT for attenuation correction although small residual artefacts were reported by both observers in a few cases.
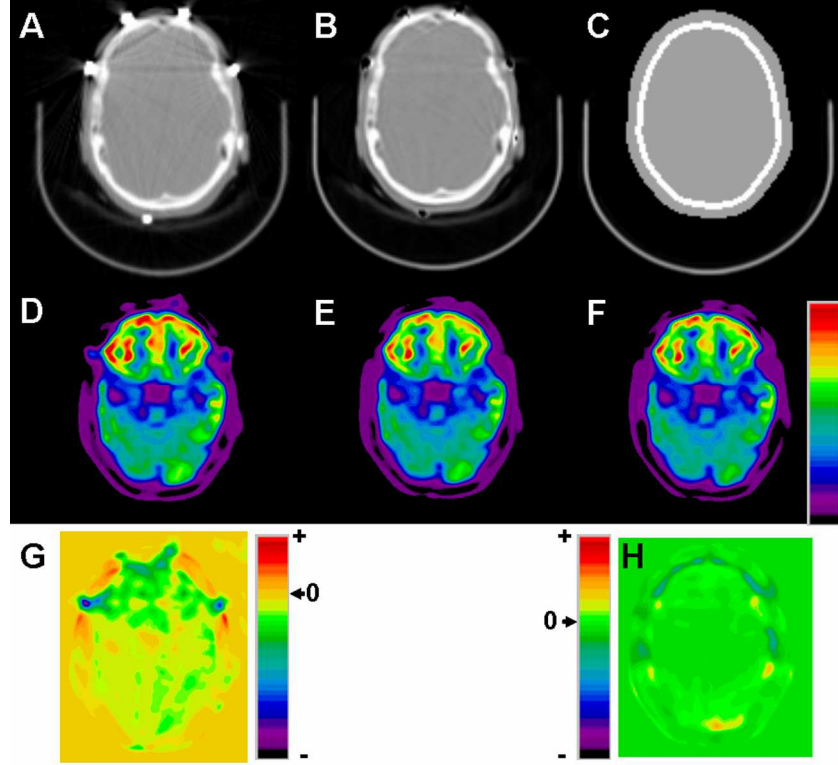

Figure 3. Results from a patient: the top row shows a transaxial slice of the attenuation correction maps while the middle row shows the corresponding reconstructed PET images. A) CT FBP reconstruction, B) CT MAR reconstruction, C) the calculated attenuation map, D) PET-FBP-AC, E) PET-MAR-AC, and F) PET-CALC-AC. The bottom row shows PET difference images: G) PET-FBP-AC – PET-MAR-AC and H) PET-CALC-AC – PET-MAR-AC.

Likewise, the PET-CALC-AC reconstructions successfully eliminated the visible metal-related hot-spot artefacts. However, invalid assumption of tissue uniformity by CALC-AC might lead to appearance of visible artefacts and significant activity quantitation bias in some regions (Zaidi *et al* 2004).

3.4 Quantitative analysis
Figure 4 shows the slopes of the regression lines and correlation coefficients between mean VOI activity values, obtained with the three attenuation correction techniques and using PET-MAR-AC as the reference. Also shown is the linear regression plot for all VOIs from all patients.
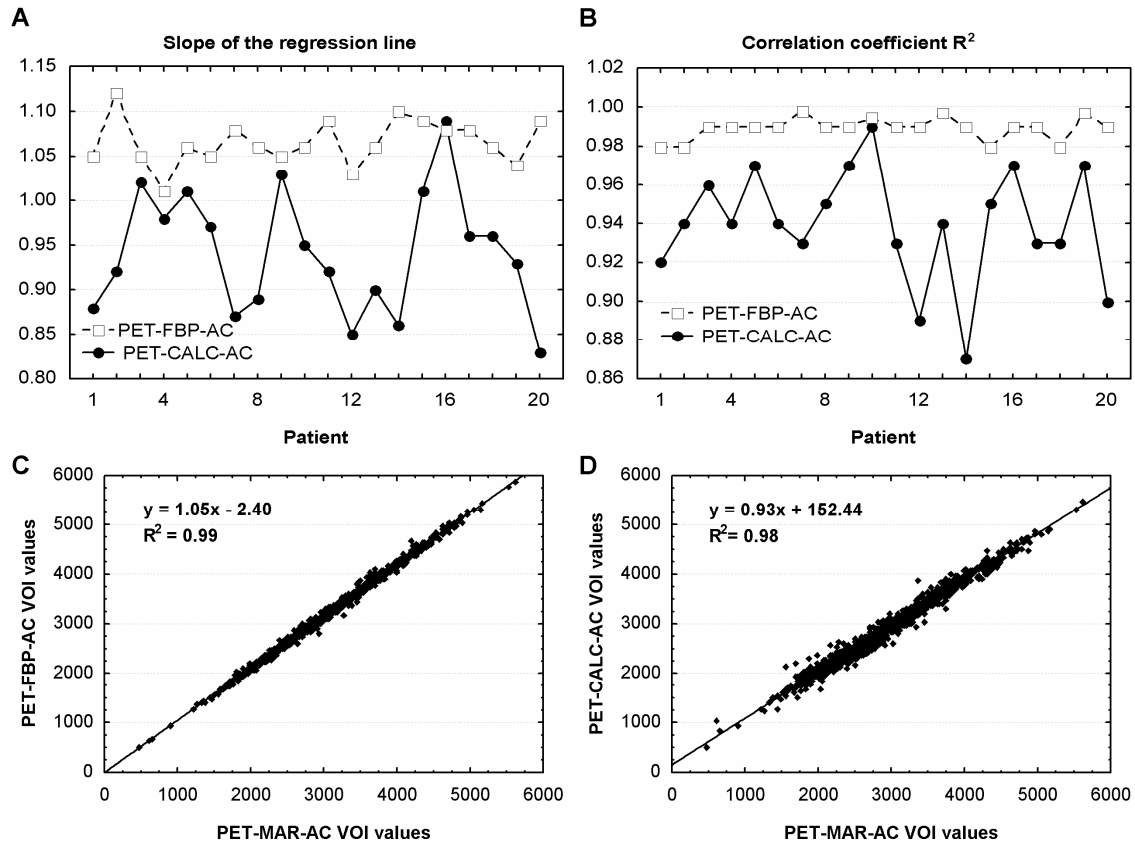
Figure 4. Plots of slopes and correlation coefficients (R^2) for each patient resulting from the linear regression analysis between PET-FBP-AC and PET-MAR-AC, and PET-CALC-AC and PET-MAR-AC. A) the slopes of the regression lines, B) the correlation coefficients. The linear regression plots of all VOIs from all patients show the correlation between C) PET-FBP-AC and PET-MAR-AC and D) PET-CALC-AC and PET-MAR-AC. The correlation coefficient and the best fit equation are also shown.

It can be seen from this figure that PET-MAR-AC and PET-FBP-AC correlate very well and that the slopes of the regression lines are close to 1. PET-MAR-AC and PET-CALC-AC correlate well but a greater variation of the slope values can be observed. This variation is also noted in the Box and Whisker plots shown in figure 5. The median of relative differences of PET-CALC-AC with respect to PET-MAR-AC per patient varies between -4.7% and 2.9%, whereas the range is limited to 4.0 through 5.5% for PET-FBP-AC compared to PET-MAR-AC.
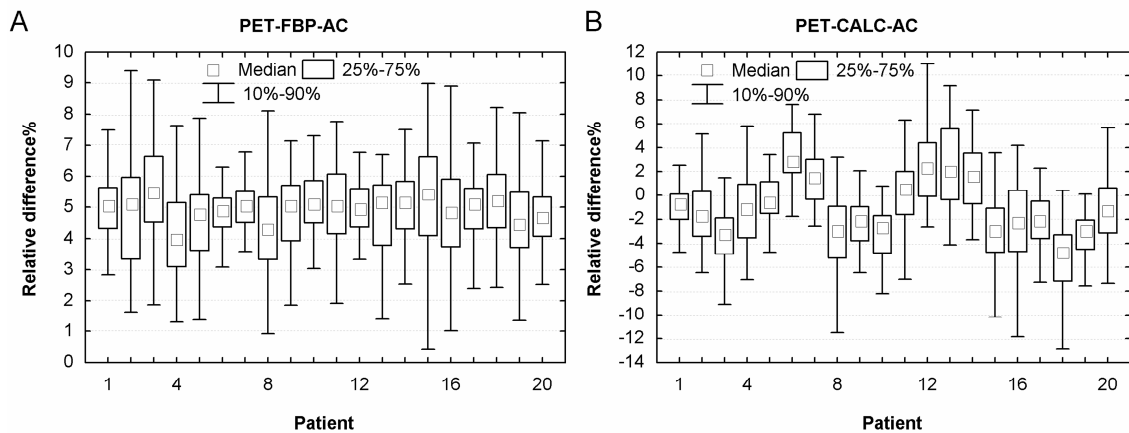

Figure 5. Box and Whisker plots showing relative differences with respect to PET-MAR-AC of A) PET-FBP-AC and B) PET-CALC-AC. The median, 10, 25, 75 and 90 percentile are calculated over all VOIs for each of the 20 patients studied.

The voxel based analysis showed an overall positive bias for the PET-FBP-AC method (figure 6) which was significant ($p < 0.05$ FWE corrected) in almost all brain voxels (data not shown). In the brain voxels, the bias was 5 to 7 % except for small regions near the electrode position and in the most anterior part of the frontal cortex. The bias in the anterior part of the frontal cortex is also shown in figure 3. The PET-CALC-AC reconstructions showed a mixed behaviour with positive bias (5-10%) in small lateral caudal regions (located in the temporal cortex and the cerebellum) and negative bias (-10% – -5%) in small regions in the anterior frontal cortex and the most posterior part of the occipital cortex (figure 7).
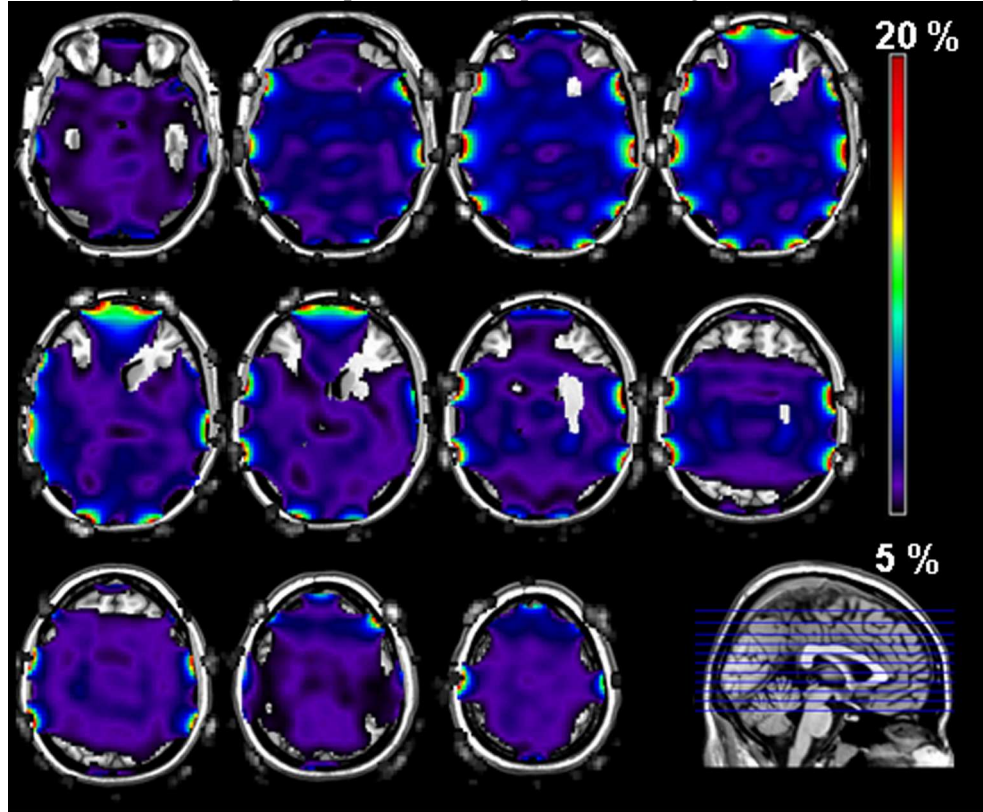

Figure 6. Quantification bias of PET-FBP-AC compared to PET-MAR-AC expressed in % change. Also the average electrode position is visualized. The quantification bias is thresholded at 5% so in the visible brain structures the bias is less than 5%. No negative bias (< -5%) was present in the brain.
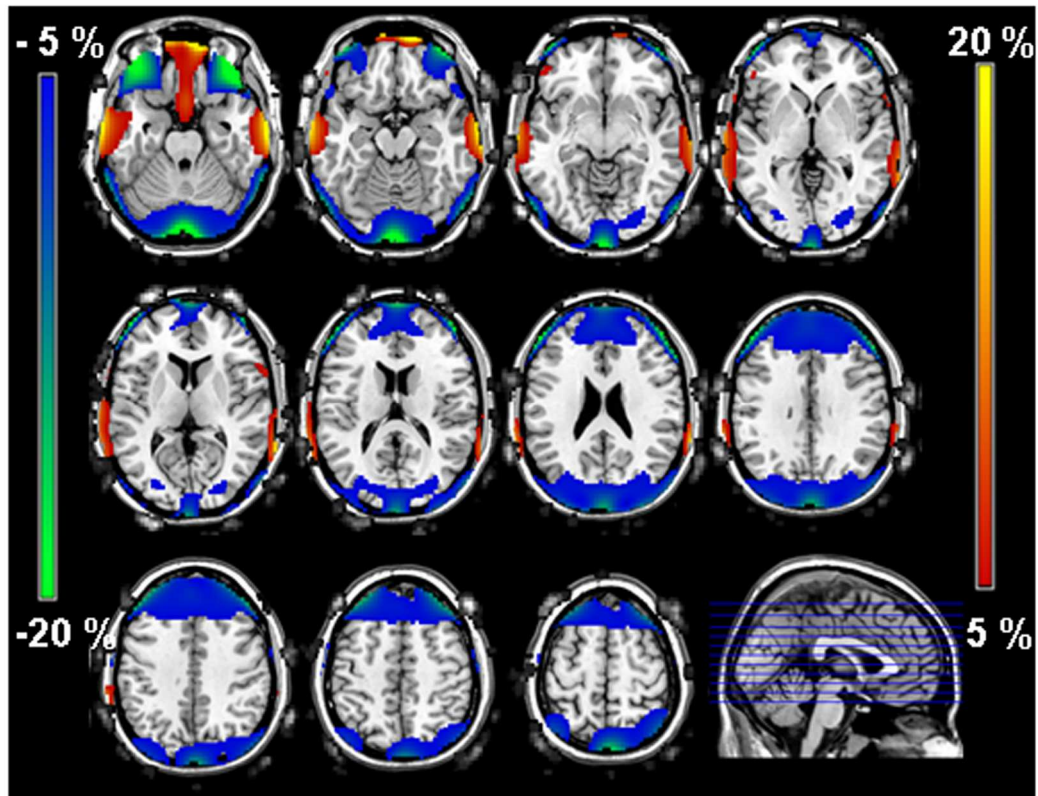
Figure 7. Quantification bias of PET-CALC-AC compared to PET-MAR-AC expressed in % change. Also the average electrode position is visualized. The quantification bias is thresholded at 5% (positive bias, colour scale red-yellow) and at -5% (negative bias, colour scale blue-green), so in the visible brain structures the bias is less than 5%.

4. Discussion

Current procedures for interpreting brain PET images in clinical diagnosis within the majority of nuclear medicine departments are still based on mere visual inspection, thereby increasing observer variance. This subjective assessment is supported in some cases by semi-quantitative statistical image analysis techniques. There are presently numerous quantitative statistical analysis methods described in the literature that are valuable in assisting in the interpretation of brain PET images (Slomka *et al* 2001; Friston *et al* 1994). It is therefore of interest to study the impact of artefacts originating from various sources. This is the aim of this study, in the particular context of artefacts arising from the presence of metallic electrodes when using CT-based PET attenuation corrected images.

In the past, one always used the PET images corrected for attenuation with the traditional PET transmission images as the gold standard in studies comparing different attenuation compensation techniques (Zaidi *et al* 2004; Montandon and Zaidi 2005). With the advent of combined PET/CT systems, which in most cases are not equipped with transmission scanning sources, it is no longer possible to use the PET transmission scan as the gold standard. Therefore, in this study, the CT images corrected for metal artefacts were used as the reference.

Except for metallic dental implants, the assessment of the impact of metallic structures on brain PET image quality and quantitative analysis has received limited attention in the literature (Zaidi *et al* 2007). A phantom study was conducted to investigate whether deep brain stimulation metallic leads can create visual and/or quantifiable artefacts in neurological PET studies (Ay and Zaidi 2007). The experiments revealed the absence of visible artefacts owing to the small size of the metallic leads. In the patient study described in this paper, the impact of EEG electrodes on the visual quality and the quantification of PET images was investigated. The presence of EEG electrodes was shown to produce local hot-spot artefacts outside the brain in CT-based attenuation corrected images and to create a significant positive bias in the brain, thus affecting the quantitative analysis of brain PET images. This is consistent with the

observations made by Kamel *et al* (2003) who studied the impact of the presence of metallic dental implants.

Two phantom experiments were conducted in which the EEG electrodes were attached on a uniform cylinder and on a plastic water bottle homogenously filled with a positron emitter. Both phantom experiments gave the same results and revealed that a zero attenuation value should be assigned to the electrodes in order to obtain similar activity concentration values in the artefactual slice and the reference artefact free PET slice. This zero attenuation value was rather unexpected and has no physical meaning. However, it can be explained by the following arguments: First, the electrodes are small (10 mm in diameter) and very thin (1 mm). However, in the CT images they are seen as small 'blobs', so their volume is greatly overestimated when a threshold for metallic structures is used. By assigning the correct attenuation value (which is unknown to us – information not disclosed by the manufacturer) to the metal pixels, the real attenuation correction factors would be greatly overestimated. This effect can be compensated by assigning a lower attenuation value to the electrodes. Second, if one looks at the CT-MAR images, one sees that in the neighbourhood of the electrodes some heightened attenuation values remain after the thresholded metallic pixels are set to zero. We believe that these small residues probably provide enough attenuation to compensate for the true attenuation by the electrodes. This means that if an exact delineation of the electrodes would be possible and if the electrodes would not create any artefacts in the CT images, the true attenuation value of the electrodes had to be used.

In the simulation study using actual brain patient data as input, the ground truth (or the exact tracer distribution) was known which allowed comparing PET-FBP-AC and PET-MAR-AC images with PET-REF. This comparison showed that the bias resulting from PET-MAR-AC was smaller than with PET-FBP-AC. In the phantom experiments, it was also shown that PET-FBP-AC suffered a positive bias of 4 to 5%, whereas PET-MAR-AC deviated by less than 1% from the reference values. Therefore it was justified to use the PET-MAR-AC as the reference for the comparative patient study. The range of the bias observed in the phantom experiments for PET-FBP-AC is also consistent with the values found in the patient study.

CT-based attenuation correction was also compared with a calculated attenuation correction method where the contour of the head was derived from the emission sinogram. Since non-uniform attenuation maps result in general in more quantitatively accurate PET images, a three-tissue model (brain tissue, skull and scalp) with a skull having a fixed thickness of 5 mm added at 10 mm depth was implemented. Ignoring the attenuation of the bed or head holder gives rise to an underestimation of activity concentration in the posterior part of the brain (Bettinardi *et al* 1994). Therefore, the attenuation of the head holder was taken into account by manually delineating the head holder in the CT images. However, as described by Michel *et al* (1989), it is possible to automate the procedure using a transmission or CT scan of the head holder and the patient bed and take into account their relative positions by reading corresponding information from the headers of the raw CT and PET projection data. The results show that the calculated attenuation correction method is a possible alternative to CT-based attenuation correction when a CT scan is not available. However, the calculated method overestimates the attenuation coefficients of the sinus and air cavities, which results in local tracer overestimation, so care has to be taken in these regions (Zaidi *et al* 2004).

A VOI- and voxel-based analysis were performed to investigate the quantitative changes induced by the use of EEG electrodes. Both analyses show the presence of a positive bias in the brain which is significant in almost all voxels when the standard CT reconstruction is used for attenuation correction. There is a quite homogenous bias of 5 to 7% throughout the brain except for some small regions near the electrodes and in the anterior part of the frontal cortex where the bias is much higher (up to 20%). It will be difficult to detect these homogenous quantitative changes by mere visual or qualitative methods, although quantitative changes in the anterior part of the frontal cortex (figure 3) were reported by the observers. However, it is unclear to what extent this bias may affect diagnosis, when the diagnostic procedure is partly based on quantitative methods. This will be the subject of further research. When comparing intra-patient data quantitatively, one has to be careful if EEG monitoring was not performed for all scans or

when the position of the electrodes varies over time. The same applies for inter-comparison of an EEG monitored patient with a database of patients where no EEG electrodes were used.

In neurological PET/CT studies, EEG electrodes give rise to local hot spots at the location of the electrodes and a positive quantification bias in the brain when no metal artefact reduction algorithm is used for the CT. The bias is rather small and is not expected to influence the diagnosis made by mere visual assessment of the brain PET images. When quantification is performed, this becomes an issue especially when comparing brain images with and without EEG monitoring.

References

Ay M R and Zaidi H 2006 Assessment of errors caused by x-ray scatter and use of contrast medium when using CT-based attenuation correction in PET *Eur. J. Nucl. Med. Mol. Imaging* **33** 1301-13

Ay M R and Zaidi H 2007 Impact of X-ray tube settings and metallic leads on neurological PET imaging when using CT-based attenuation correction *Nucl. Instr. Meth. Phys. Res. A* **571** 411-14

Bettinardi V, Gilardi M C, Cargnel S, Rizzo G, Teräs M, Striano G and Fazio F 1994 A hybrid method of attenuation correction for positron emission tomography brain studies *Eur. J. Nucl. Med.* **21** 1279-84

Carney J P J, Townsend D, Rappoport V and Bendriem B 2006 Method for transforming CT images for attenuation correction in PET/CT imaging *Med. Phys.* **33** 976-83

Coolens C and Childs P J 2003 Calibration of CT Hounsfield units for radiotherapy treatment planning of patients with metallic hip prostheses: the use of the extended CT-scale *Phys. Med. Biol.* **48** 1591-603

Defrise M, Kinahan P E, Townsend D W, Michel C, Sibomana M and Newport D F 1997 Exact and approximate rebinning algorithms for 3-D PET data *IEEE Trans. Med. Imaging* **16** 145-58

De Man B, Nuyts J, Dupont P, Marchal G and Seutens P 1999 Metal streak artifacts in computed tomography: a simulation study *IEEE Trans. Nucl. Sci.* **46** 691-96

De Man B, Nuyts J, Dupont P, Marchal G and Suetens P 2000 Reduction of metal streak artifacts in x-ray computed tomography using a transmission maximum a posteriori algorithm *IEEE Trans. Nucl. Sci.* **47** 977-81

Friston K J, Holmes A P, Worsley KJ, Poline J-P, Frith C D and Frackowiak R S J 1994 Statistical parametric maps in functional imaging: a general linear approach. *Hum Brain Mapp* **2** 189-210

Ghoorun S, Baete K, Nuyts J, Groenewald W and Dupont P 2006 The influence of attenuation correction and reconstruction techniques on the detection of hypo-perfused lesions in brain SPECT images *Nucl. Med. Commun.* **27** 765-72

Goerres G W, Ziegler S I, Burger C, Berthold T, von Schulthess G K and Buck A 2003 Artifacts at PET and PET/CT caused by metallic hip prosthetic material *Radiology* **226** 577-84

Hudson H M and Larkin R S 1994 Accelerated image reconstruction using ordered subsets of projection data *IEEE Trans. Med. Imaging* **13** 601-9

Kalender W A, Hebel R and Ebersberger J 1987 Reduction of CT artifacts caused by metallic implants *Radiology* **164** 576-7

Kamel E M, Burger C, Buck A, von Schulthess G K and Goerres G W 2003 Impact of metallic dental implants on CT-based attenuation correction in a combined PET/CT scanner *Eur. Radiol.* **13** 724-28

Kinahan P E, Hasegawa B H and Beyer T 2003 X-ray based attenuation correction for positron emission tomography/computed tomography scanners *Semin. Nucl Med.* **33** 166-79

Lemmens C, Faul D, Hamill J, Stroobants S and Nuyts J 2006 Suppression of metal streak artifacts in CT using a MAP reconstruction procedure *IEEE NSS-MIC Conference Record* **6** 3431-37

Lemmens C, Faul D and Nuyts J 2008 Suppression of metal artifacts in CT using a reconstruction procedure that combines MAP and projection completion *IEEE Trans. Med. Imaging* in revision

Liang Z, Jaszczak R, Coleman R and Johnson V 1991 Simultaneous reconstruction, segmentation, and edge enhancement of relatively piecewiece continuous images with intensity-level information *Med. Phys.* **18** 394-401

Maes F, Collignon D, Vandermeulen D, Marchal G and Seutens P 1997 Multimodality image registration by maximization of mutual information *IEEE Trans. Med. Imaging* **16** 187-98

Mahnken A H, Raupach R, Wildberger J E, Jung B, Heussen N, Flohr T G, Günther R W and Schaller S 2003 A new algorithm for metal artefact reduction in computed tomography. In vitro and in vivo evaluation after total hip replacement *Invest. Radiol.* **38**, 769-75

Michel C, Bol A, De Volder A G and Goffinet A M 1989 Online brain attenuation correction in PET: towards a fully automated data handling in a clinical environment *Eur. J. Nucl. Med.* **15** 712-18

Montandon M-L and Zaidi H 2005 Atlas-guided non-uniform attenuation correction in cerebral 3D PET imaging *NeuroImage* **25** 278-86

Nuyts J, Dupont P, Stroobants S, Benninck R, Mortelmans L and Suetens P 1999 Simultaneous maximum a posteriori reconstruction of attenuation and activity distributions from emission sinograms *IEEE Trans. Med. Imaging* **18** 393-403

Qi J and Leahy R M 2006 Iterative reconstruction techniques in emission computed tomography *Phys. Med. Biol.* **51** R541-78

Radau P E, Slomka P J, Julin P, Svensson L and Wahlund L-O 2001 Constrained localized-warping-reduced registration errors due to lesions in functional neuroimages, *Proc. SPIE* **4322** 588-601

Slomka P J, Radau P, Hurwitz G A and Dey D 2001 Automated three-dimensional quantification of myocardial perfusion and brain SPECT *Comput. Med. Imaging Graph.* **25** 153-64

Siegel S and Dahlbom M 1992 Implementation and evaluation of a calculated attenuation correction for PET *IEEE Trans. Nucl. Sci.* **39** 1117-21

Stodilka R Z, Kemp B J, Prato F S and Nicholson R L 1998 Importance of bone attenuation in brain SPECT quantification *J. Nucl. Med.* **39** 190-7

Stodilka R Z, Kemp B J, Prato F S, Kertesz A, Kuhl D and Nicholson R L 2000 Scatter and attenuation correction for brain SPECT using attenuation distributions inferred from a head atlas *J. Nucl. Med.* **41** 1569-78

Studholme C, Hill D L G and Hawkes D J 1999 An overlap invariant entropy measure of 3D medical image alignment *Pattern Recogn.* **32** 71-86

Watson C C 2000 New, faster, image-based scatter correction for 3D PET *IEEE Trans. Nucl. Sci.* **47** 1587-94

Weinzapfel B T and Hutchins G D 2001 Automated PET attenuation correction model for functional brain imaging *J. Nucl. Med.* **42** 483-91

Zaidi H, Montandon M-L and Slosman D O 2004 Attenuation compensation in cerebral 3D PET: effect of the attenuation map on absolute and relative quantitation *Eur. J. Nucl. Med. Mol. Imaging* **31** 52-63

Zaidi H, Montandon M-L and Meikle S 2007 Strategies for attenuation compensation in neurological PET studies *NeuroImage* **34** 518-41

Zeng G L, Gullberg G T, Tsui B M W and Terry J A 1991 Three-dimensional iterative reconstruction algorithms with attenuation and geometric point response correction *IEEE Trans. Nucl. Sci.* **38** 693-701